PAPER

A highly selective and sensitive fluorescent chemosensor for Zn^{2+} based on a diarylethene derivative†

Erting Feng, Yayi Tu, Congbin Fan, ID * Gang Liu and Shouzhi Pu*

A promising photochromic fluorescent chemosensor **1o** linked with Schiff base unit was synthesized. It displayed outstanding photochromism and a superb fluorescence turn-on response toward Zn^{2+}. Upon the addition of Zn^{2+} to **1o**, the fluorescent color of the solution obviously changed from blue to bright green with a 27-fold fluorescent intensity increase. The combination of **1o**–Zn^{2+} with 1 : 1 stoichiometry was verified by Job's plot and MS analysis. The detection limit for **1o** toward Zn^{2+} was measured to be 8.10×10^{-8} M. Furthermore, logic gate research was established with Zn^{2+}, UV and visible light as input signals and the emission intensity as the output signal.

1. Introduction

It is well known that zinc is the second most plentiful transition metal in cells as well as the requisite ingredient to maintain life.[1] Many research studies reveal that Zn^{2+} plays a crucial role in a number of biological metabolic processes, such as enzyme regulation, neural signal modulation and apoptosis.[2–4] Free Zn^{2+} exist in some tissues, acting as signal transporters for nerve transmission and necrocytosis.[5,6] Micro quantities of zinc are essential with about 2–4 g distributed over the human body,[7,8] but its excess may damage the organism,[9,10] for instance, overmuch Zn^{2+} in the body will suppress the ingestion of other essential trace metal ions such as Fe^{3+} and Cu^{2+}.[11,12] The inconsistency of Zn^{2+} concentration with the normal levels in the human body will cause diverse diseases, *e.g.*, diabetes, Alzheimer's disease, epilepsy and so forth.[13,14] Hence, studies focused on Zn^{2+} detection are of great significance. Up to now, conventional ways used for identifying Zn^{2+}, such as atomic absorption spectrometry[15] and inductively coupled plasma mass spectrometry,[16] generally require precision instruments, high cost and inconvenient operation. Therefore, it is worthwhile to develop new methods with low cost, easy operability and high selectivity for Zn^{2+} detection.

In recent decades, fluorescent chemosensors have developed rapidly to monitor special species in numerous fields such as environmental analysis and clinical diagnosis[17,18] due to its high selectivity, efficient sensitivity, real-time detection and easy

Jiangxi Key Laboratory of Organic Chemistry, Jiangxi Science and Technology Normal University, Nanchang 330013, P. R. China. E-mail: congbinfan@163.com; pushouzhi@vip.163.com; Fax: +86 791 83805212; +86 791 83831996; Tel: +86 791 83805212; +86 791 83831996

sample preparation.[19,20] Up to now, a considerable amount of fluorescent sensors targeting transition and heavy metal ions with transient response and splendid selectivity have been reported.[21–24] As known to all, quinoline as an important fine chemical raw material, mainly used for the synthesis of pharmaceutical, dyes and a variety of chemical catalysts.[25–29] On the other hand, an increasing number of photochromic molecular systems have been used as fluorescent probes to detect metal ions in recent years.[30–32] Among these photochromic materials, diarylethenes have attracted increasing attention due to its excellent anti-fatigue for switching the intensity of fluorescent emission as well as its potential applications in molecular switching devices.[33,34] Heretofore, a variety of Zn^{2+} fluorescence chemosensors decorated with diarylethenes have been reported.[35,36] However, these sensors either have poor detection limits or disturbances of other metal ions, such as Cd^{2+} exhibiting similar chemical properties.[37,38]

Herein, we designed a novel fluorescent turn-on chemosensor (**1o**) based on a diarylethene derivative for detecting Zn^{2+} with high selectivity and sensitivity. Besides, the recognition of Zn^{2+} did not have any disturbance from Cd^{2+}. The synthetic route and photochromism of target sensor **1o** were shown in Scheme 1. Related substances in this paper are characterized by ^1H NMR, ^{13}C NMR and mass spectrum as seen in the ESI (Fig. S9–S17†).
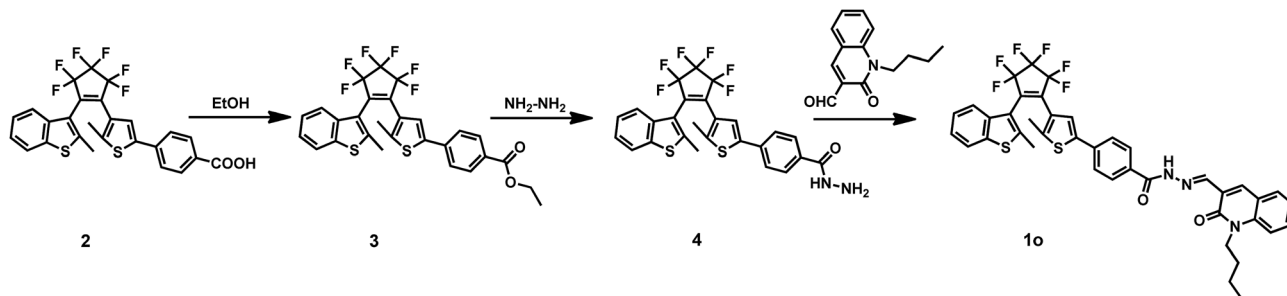
2. Experimental

2.1 General methods

All reagents were analytical grade without further purification and all other solvents used in properties testing were spectroscopic grade. The solutions of the metal ions were prepared from the nitrates (0.1 M) of Cu^{2+}, Zn^{2+}, Cd^{2+}, Fe^{3+}, Pb^{2+}, Ca^{2+}, Co^{2+}, Cr^{3+}, Ni^{2+}, Mg^{2+}, Sr^{2+} and Al^{3+}, except for K^+, Ba^{2+}, Mn^{2+},

Scheme 1   The synthesis of compound **1o**.

Hg^{2+} (their counter ions were chloride ions), in distilled water (2 mL). ^1H NMR and ^{13}C NMR spectra were recorded on a Bruker AV400 (400 MHz) spectrometer with tetramethylsilane (TMS) as its internal standard. Melting points were obtained on a WRS-1B melting point apparatus. Mass spectra were measured on an AB SCIEX Triple TOF 4600 instrument. Elemental analysis was performed with a PE CHN 2400 analyzer. The fluorescence quantum yield was recorded with an Absolute PL Quantum Yield Spectrometer QY C11347-11. UV-Vis absorption spectra were measured on an Agilent 8453 UV-Vis spectrometer. Fluorescence spectra were recorded with a Hitachi F-4600 fluorescence spectrophotometer. Photo-irradiation was performed with an SHG-200 UV lamp, Cx-21 ultraviolet fluorescence analysis cabinet and a BMH-250 visible lamp.

2.2   Synthesis of compound 3

The synthetic route was shown in Scheme 1. Compound **2** (ref. 39) (0.54 g, 1 mmol) and a catalytic amount of acetic acid were dissolved in anhydrous ethanol (10 mL). The solution was heated to reflux for 6 h until no compound **2** was detected by TLC silica gel plate detection. Then the solvent was removed under reduced pressure, and the mixture was extracted with dichloromethane. The organic layer was washed with brine and water, dried over anhydrous Na_2SO_4 and evaporated to dryness under reduced pressure to obtain the crude product **3**, which was purified by separating on a silica gel chromatography column with petroleum ether/ethyl acetate (10/1) as the eluent to obtain the compound **3** (0.51 g, yield: 90%). ^1H NMR (400 MHz, $CDCl_3$, TMS), δ (ppm): 1.39 (t, 3H, –CH_3), 1.97 (s, 3H, –CH_3), 2.31 (s, 3H, –CH_3), 4.35–4.40 (m, 2H, –CH_2–), 7.25 (s, 1H, Ar-H), 7.29–7.37 (m, 2H, Ar-H), 7.45 (d, 2H, Ar-H), 7.57 (d, 1H, Ar-H), 7.73 (d, 1H, Ar-H), 7.99 (d, 2H, Ar-H). ^{13}C NMR (100 MHz, $CDCl_3$, TMS), δ (ppm): 14.42, 14.91, 61.14, 120.37, 122.17, 122.21, 124.14, 124.69, 125.10, 125.26, 125.64, 129.75, 130.38, 137.43, 138.41, 140.69, 142.59, 143.09, 166.17. Anal. calcd for $C_{28}H_{20}F_6O_2S_2$ (%): C, 59.36; H, 3.56. Found: C, 59.31; H, 3.59. ESI-MS: $m/z = 565.0721\ [M - H]^-$ (calcd 565.0731).

2.3   Synthesis of compound 4

Compound **3** (0.57 g, 1 mmol) was suspended in anhydrous ethanol (10 mL) and then hydrazine hydrate (99%, 2 mL) was added dropwise. The mixture was heated at 353 K and stirred for 12 h. After removing the solvent by evaporation under reduced

pressure, the crude product **4** was purified by column chromatography using petroleum ether/ethyl acetate (3/1, 1% Et_3N) as the eluent to acquire the compound **4** (0.25 g, yield: 45%). ^1H NMR (400 MHz, $CDCl_3$, TMS), δ (ppm): 1.96 (s, 3H, –CH_3), 2.31 (s, 3H, –CH_3), 3.49 (s, 2H, –NH_2), 7.25 (s, 1H, Ar-H), 7.30–7.38 (m, 3H, Ar-H), 7.48 (d, 2H, Ar-H), 7.57 (d, 1H, Ar-H), 7.71–7.76 (m, 3H, Ar-H). ^{13}C NMR (100 MHz, $CDCl_3$, TMS), δ (ppm): 14.76, 14.84, 120.24, 122.05, 122.09, 122.15, 123.77, 124.62, 125.02, 125.42, 125.49, 127.78, 136.46, 138.24, 138.32, 140.49, 142.56, 142.90, 167.86. Anal. calcd for $C_{26}H_{18}F_6N_2OS_2$ (%): C, 56.52; H, 3.28; N, 5.07. Found: C, 56.44; H, 3.31; N, 5.09. ESI-MS: $m/z = 551.0684\ [M - H]^-$ (calcd 551.0686).

2.4   Synthesis of compound 1o

Compound **4** (0.11 g, 0.2 mmol) was suspended in absolute ethanol (10 mL), followed by the addition of 1-butyl-2-oxo-1,2-dihydroquinoline-3-carbaldehyde (0.045 g, 0.2 mmol) and a catalytic amount of acetic acid. The mixture was stirred at 353 K for 12 h to complete the reaction. Then the solution was cooled to room temperature and put in a refrigerator overnight. A yellow solid precipitation was observed and then washed with absolute methanol (10 mL × 3) to afford the compound **1o** (0.091 g, yield: 60%). Mp: 342–343 K. ^1H NMR (400 MHz, CD_2Cl_2, TMS), δ (ppm): 0.88 (t, 3H, –CH_3), 1.34 (m, 2H, –CH_2–), 1.59 (m, 2H, –CH_2–), 1.90 (s, 3H, –CH_3), 2.26 (s, 3H, –CH_3), 4.16 (t, 2H, –CH_2–), 7.16–7.30 (m, 5H, Ar-H), 7.43–7.53 (m, 4H, Ar-H), 7.64 (d, 1H, Ar-H), 7.69 (d, 1H, Ar-H), 7.78 (d, 2H, Ar-H), 8.47 (s, 1H, –CH=N–), 8.61 (s, 1H, Ar-H), 9.89 (s, 1H, –NH–). ^{13}C NMR (100 MHz, CD_2Cl_2, TMS), δ (ppm): 14.19, 15.24, 20.84, 30.13, 43.05, 44.16, 114.95, 115.46, 120.62, 121.17, 122.58, 122.76, 123.07, 124.04, 124.57, 125.20, 125.58, 126.02, 130.90, 132.10, 132.80, 133.45, 138.79, 139.01, 140.29, 161.57. Anal. calcd for $C_{40}H_{31}F_6N_3O_2S_2$ (%): C, 62.90; H, 4.09; N, 5.50. Found: C, 62.83; H, 4.12; N, 5.56. ESI-MS: $m/z = 762.1666\ [M - H]^-$ (calcd 762.1684).

3.   Results and discussion

3.1   Photochromic and fluorescent properties of compound 1o

The photochromism of compound **1o** (20 μM in THF) at room temperature was shown in Fig. 1a. In the initial state of **1o**, two split absorption peaks were observed at 341 nm and 382 nm, which can be ascribed to $\pi \rightarrow \pi^*$ transition,[40,41] and the solution
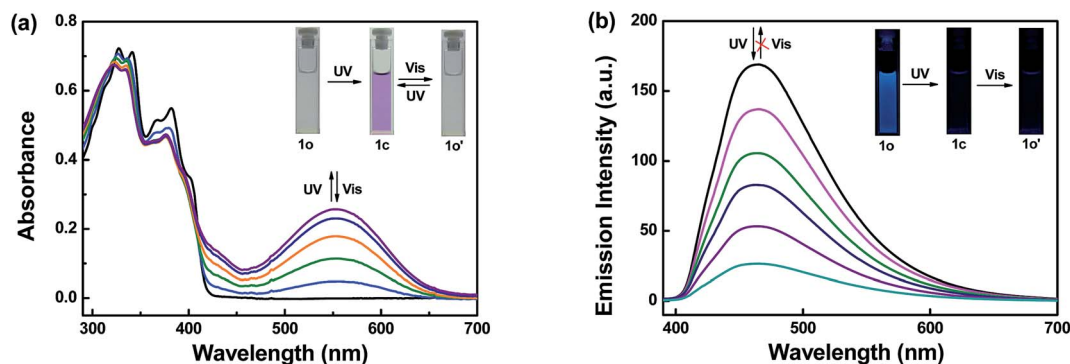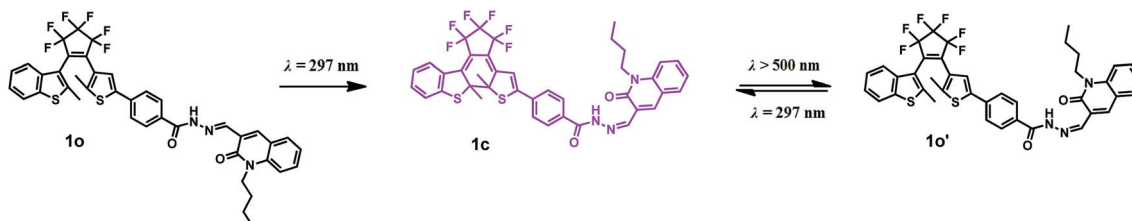
Fig. 1 Upon irradiation with UV-Vis light: (a) absorption spectra changes of **1o** (20 μM in THF), (b) fluorescence spectra changes of **1o** (20 μM in THF).

Scheme 2 The photochromism and plausible C=N isomerization of compound **1o**.

was colorless. Upon irradiation with 297 nm light, two sharp bands at 341 nm and 382 nm gradually decreased and a new broad band at 555 nm was observed, indicating the formation of closed ring isomer **1c**. When the photostationary state (PSS) was reached, a clear isosbestic spot at 410 nm was observed, and the solution changed from colorless to purple. Relatively, when irradiated with appropriate visible light ($\lambda > 500$ nm), the absorption spectrum intensity at 555 nm recovered to the original state due to the ring cleavage reaction. While in ultraviolet region, a new status different from **1o** was reached which may because of C=N isomerization (Fig. S1†). A dissimilar open loop isomer (**1o′**) was generated as shown in Scheme 2. Anti-fatigue tests ($\lambda = 555$ nm) were carried out through 15 cycles of coloration–decoloration (Fig. S2†), and the result indicated that **1o** had prominent fatigue resistance. Fig. 1b shows the fluorescence spectra changes of **1o** (20 μM in THF) upon irradiation with UV-Vis light. The original state of **1o** displayed weak fluorescence at 464 nm when excited at 380 nm with a low quantum yield ($\Phi = 0.008$). Upon irradiation with 297 nm light, the fluorescence emission peak gradually decreased due to the generation of non-fluorescent isomer **1c**.[42] When the PSS was reached, the fluorescent color changed from blue to darkness. Unfortunately, when irradiated with visible light ($\lambda > 500$ nm), the fluorescence intensity hardly changed which may be ascribed to the isomerization of C=N bond in excited state.

3.2 Absorption and fluorescence spectra responses of 1o toward Zn²⁺

The detection of Zn²⁺ by sensor **1o** was initially assessed by the UV-Vis spectra. The absorption spectra changes of **1o** (20 μM in

THF) in the presence of different equivalents of Zn²⁺ (0–1.2 equiv.) were exhibited in Fig. 2a. With addition of increased amount of Zn²⁺, the first band around 341 nm gradually reduced and a new absorption band at 411 nm obviously increased. A plot of absorbance intensity depending on the equivalents of Zn²⁺ showed that the absorption intensity at 411 nm gradually increased until the amount of Zn²⁺ reached 1.2 equivalents (Fig. S3†). Meanwhile, a clear isosbestic point at 369 nm was observed, demonstrating the formation of **1o**–Zn²⁺ complex. The solution color changed from colorless to yellow, which was consistent well with the absorption spectra changes. Upon irradiation with 297 nm light, the photochromic properties of **1o**–Zn²⁺ were performed in Fig. 2b, a new absorption broad band emerged at 557 nm. At the PSS, the solution color became brown from yellow. Reversely, upon irradiation with visible light ($\lambda > 500$ nm), the absorption spectrum of **1c**–Zn²⁺ was restored to its incipient state of **1o**–Zn²⁺ and the solution color returned from brown to yellow.

The fluorescence response experiments were ulteriorly carried out to investigate the interaction between **1o** (20 μM in THF) and Zn²⁺ by adding various equivalents of Zn²⁺ (0–1 equiv.) to **1o** (Fig. 3a). The fluorescence titration experiments showed that the maximum emission intensity was achieved when 1 equivalent of Zn²⁺ was added to the solution, excited by 380 nm light (Fig. S4†). As can be seen from above that the emission intensity of **1c** can not recover to that of **1o** due to the free rotation around C=N bond. The isomerization of C=N bond was always considered to be the predominant decay process in excited state.[24,43] With the addition of Zn²⁺, the emission intensity dramatically increased associated with a red shift from 464 nm to 513 nm. When the amount of Zn²⁺ reached
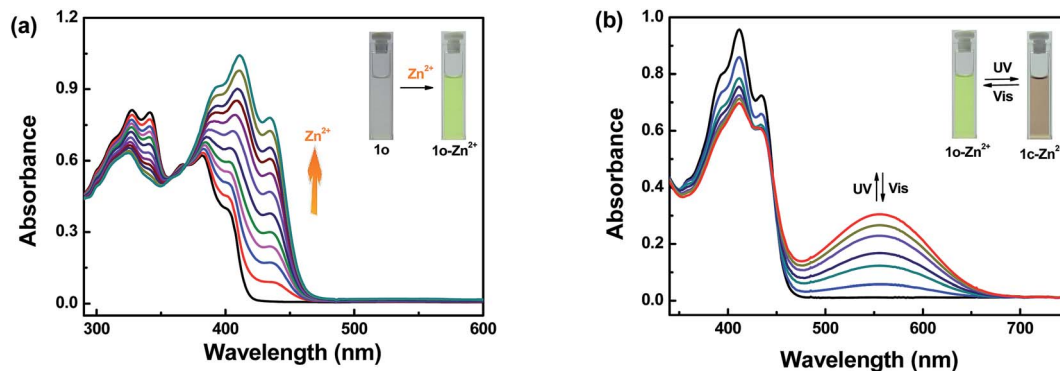
Fig. 2 (a) Absorption spectra changes of **1o** (20 μM in THF) induced by Zn^{2+} ions (0−1.2 equiv.). (b) Absorption spectra changes of **1o**−Zn^{2+} (20 μM in THF) upon irradiation with UV-Vis light.

1 equivalent, the fluorescence intensity achieved its maximum with a high quantum yield ($\Phi = 0.220$) which is 27-fold larger than that of **1o**. At the same time, the fluorescent color apparently changed from blue to bright green, which was coincident with the changes in the fluorescence spectra. The formation of complex **1o**–Zn^{2+} should be responsible for these phenomena. By combining with Zn^{2+}, the C=N isomerization was suppressed, and the increased rigidity of the molecule leaded to chelation enhanced fluorescence (CHEF), thereby realizing the fluorescence enhancement of complex **1o**–Zn^{2+}.[44-47]

Noteworthily, because of the inhibition of C=N isomerization, the chelate **1o**–Zn^{2+} showed prominent fluorescence switch performance by UV-Vis light irradiation (Fig. 3b) as compared with the probe **1o** (Fig. 1b). Upon irradiation with 297 nm light, the emission peak gradually decreased due to the formation of closed-ring isomer **1c**–Zn^{2+}.[42] The fluorescent color changed from bright green to dark green in the wake of the fluorescence intensity reached the minimum. Relatively, the fluorescence spectrum of **1c**–Zn^{2+} recovered to its initial state of **1o**–Zn^{2+} upon irradiation with visible light ($\lambda > 500$ nm). The fluorescence spectral responses among closed-ring isomer **1c** and Zn^{2+} were further studied as shown in Fig. 3c. With the addition of Zn^{2+} (0–1 equiv.), the emission intensity was obviously enhanced accompanied by a red shift from 464 nm to 513 nm. The C=N
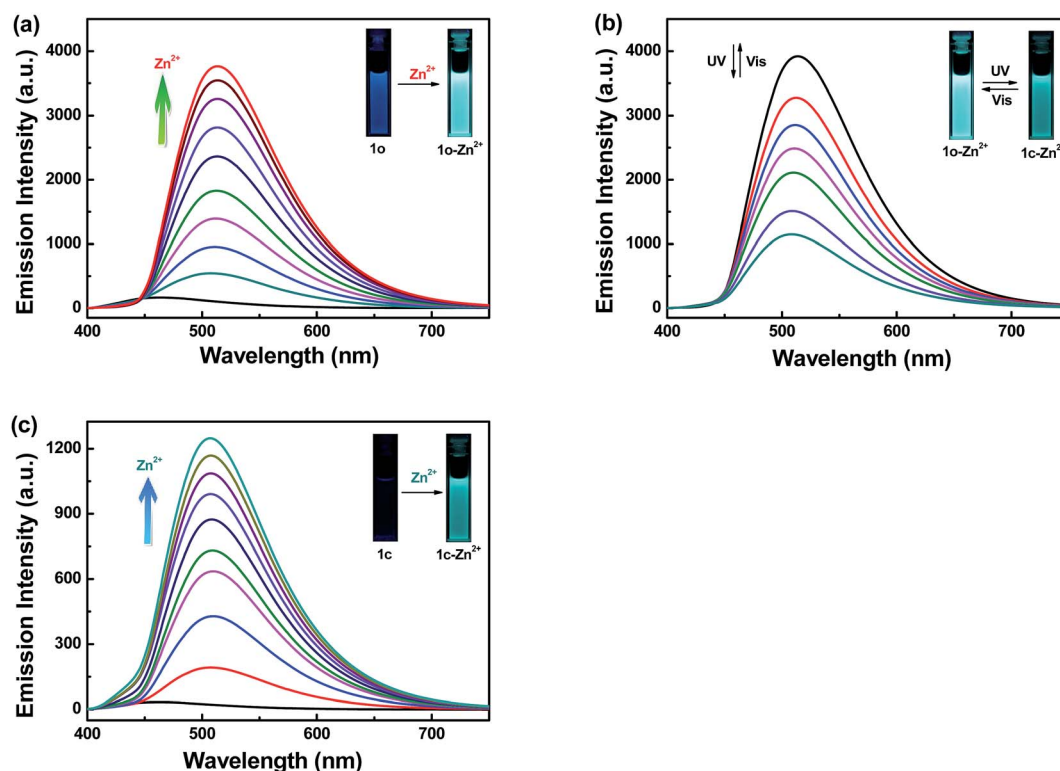

Fig. 3 (a) Fluorescence spectra changes of **1o** (20 μM in THF) induced by Zn^{2+} (0−1 equiv.). (b) Fluorescence spectra changes of **1o**−Zn^{2+} (20 μM in THF) upon irradiation with UV-Vis light. (c) Fluorescence spectra changes of **1c** (20 μM in THF) induced by Zn^{2+} (0−1 equiv.).
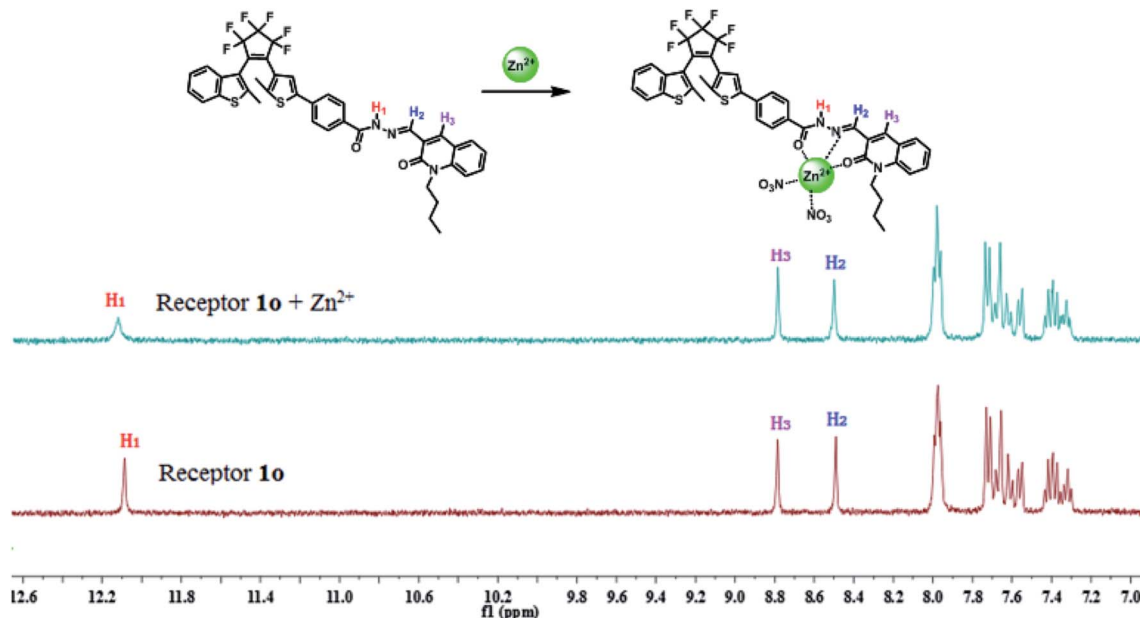
Fig. 4 ^{1}H NMR (DMSO-d_6, 400 MHz) spectra changes of receptor **1o** in the presence of 1 equivalent of Zn^{2+}.

isomerization was prohibited through the interaction between **1c** and Zn^{2+}, indicating that Zn^{2+} induced fluorescence turn-on behavior. When the amount of Zn^{2+} reached 1 equivalent, the fluorescence intensity reached its maximum ($\Phi = 0.030$), and meanwhile, the fluorescent color changed from darkness to dark green.

To get a further insight into the binding mode of complex **1o**–Zn^{2+}, the Job's plot analysis experiment was implemented by the fluorescence titration in THF solution, which distinctly shows a 1 : 1 stoichiometry between Zn^{2+} and **1o** (Fig. S5†). The association constant (K_a) for the complex **1o**–Zn^{2+} was determined by

the corresponding fluorescence titration data in 1 : 1 binding equation as 2.27×10^4 M^{-1} (Fig. S6†). Besides, the detection limit (LOD) of **1o** to Zn^{2+} was evaluated to be 8.10×10^{-8} M based on LOD = $3\sigma/s$, where "σ" is the standard deviation of blank sample, and "s" is the slope between the fluorescence intensity *versus* Zn^{2+} concentration (Fig. S7†).[48] Mass spectrum and ^{1}H NMR spectra were utilized to further verify the binding fashion of receptor **1o** toward Zn^{2+}. The peak located at $m/z = 950.4967$ was coincided well with the ensemble $[\mathbf{1o} + \text{Zn}^{2+} + 2\text{NO}_3^- - \text{H}^+]^-$, proving the existence of complex **1o**–Zn^{2+} with a 1 : 1 stoichiometry (Fig. S8†). Fig. 4 shows the ^{1}H NMR spectra changes upon the addition of
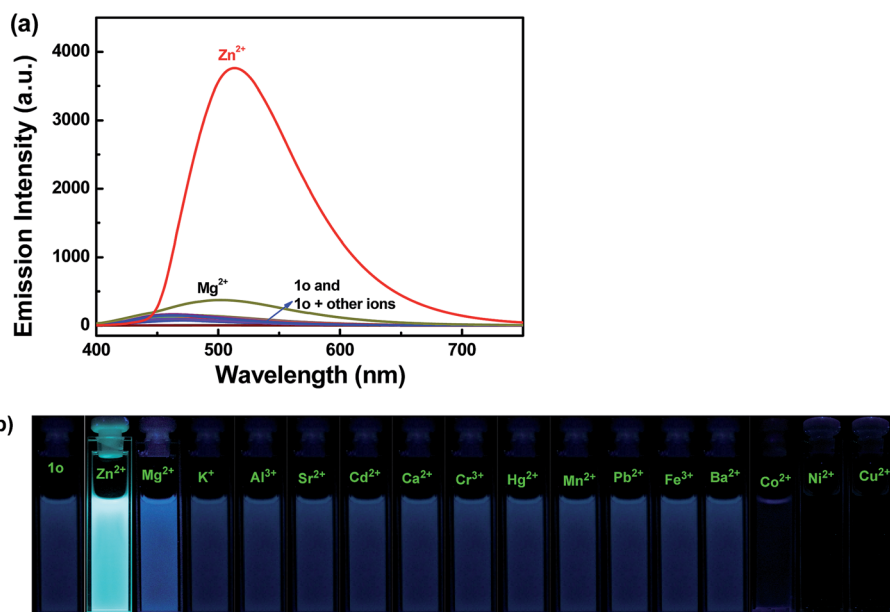

Fig. 5 Upon addition various metal ions to **1o** (20 μM in THF): (a) fluorescence emission spectra, (b) fluorescent photos.

Zn^{2+} to the DMSO-d_6 solution of **1o**. As can be seen that the signal of the –NH proton at 12.087 ppm became broad and moved slightly toward the low field region in the presence of 1 equivalent of Zn^{2+}. Besides, the signal intensity at 8.490 ppm belonging to –N=CH proton was slightly weaker. In view of above mentioned changes, we proposed the complexation between receptor **1o** and Zn^{2+} was achieved through two oxygen atoms of the carbonyl groups (C=O) as well as one nitrogen of the imine nitrogen group (–CH=N) as demonstrated in Fig. 4.

The fluorescence selectivity of **1o** (20 μM in THF) toward different metal ions was investigated as shown in Fig. 5. Receptor **1o** showed very weak fluorescence intensity upon excitation at 380 nm. After adding a variety of metal ions (Cu^{2+}, Zn^{2+}, Cd^{2+}, Fe^{3+}, Pb^{2+}, Ca^{2+}, Co^{2+}, Cr^{3+}, Ni^{2+}, Mg^{2+}, Sr^{2+}, Al^{3+}, K^+, Ba^{2+}, Mn^{2+} and Hg^{2+}, 1 equiv. each), only Zn^{2+} caused a prominent fluorescence enhancement centered at 513 nm, indicating an efficient fluorescence turn-on behavior. Besides, it is imperative to note that the recognition of **1o** toward Zn^{2+} was not subject to any interference from Cd^{2+}. Fig. 5b shows the fluorescent photos of **1o** upon addition of various metal ions in THF solution. The fluorescent color of **1o**–Zn^{2+} was obviously bright green, indicating that sensor **1o** could be used for detecting Zn^{2+} with high selectivity.

4. Logic gate research

As mentioned above, sensor **1o** (20 μM in THF) exhibited significant fluorescence turn-on response upon the addition of Zn^{2+}, and then can be further adjusted by UV-Vis light irradiation. The selective fluorescence "on–off" conversion of receptor **1o** stimulated by Zn^{2+} and UV-Vis light inspired us to investigate its feasible application in the field of logic gate (Fig. 6). In this research, the fluorescence intensity of **1o** was regarded as the initial value, and only if the emission intensity was 10-fold larger than the initial value, the output signal was considered "on" (readout "1"). Thus, the signal turn-on behavior occurred only when Zn^{2+} was chelated

with the open ring isomer **1o**. In all other input combinations, the output signal remained in "off" state (readout "0").

5. Conclusion

In summary, a new photochromic fluorescent probe **1o** was synthesized for the first time. As a diarylethene derivative, probe **1o** not only revealed splendid photochromic properties, but also exhibited superb fluorescence selectivity and high sensitivity toward Zn^{2+}. Upon excitation at 380 nm, only Zn^{2+} induced significant fluorescence enhancement with 27-fold fluorescent intensity increase, and simultaneously, the fluorescent color of **1o** obviously changed from blue to bright green. Noteworthily, the selective fluorescence turn-on behavior caused by Zn^{2+} had no interference from Cd^{2+}. The detection limit was as low as 8.10×10^{-8} M. This fluorescence enhancement was ascribed to the inhibition of C=N isomerization and CHEF between receptor **1o** and Zn^{2+}. In addition, the logic gate study was established based on the fluorescence intensity of **1o** could be modulated by Zn^{2+}, UV and visible light.

Conflicts of interest

There are no conflicts to declare.
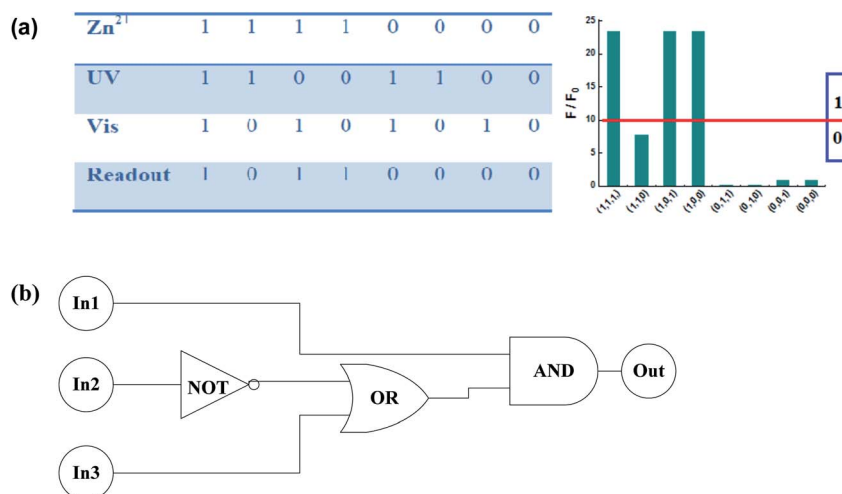
Acknowledgements

Fig. 6 Zn^{2+} (In 1), $\lambda = 297$ nm light (In 2) and $\lambda > 500$ nm light (In 3) as inputs and their corresponding logic readout in the form of bar graph representation (a) and the combinational logic circuit (b).

References

1 J. M. Berg and Y. G. Shi, *Science*, 1996, **271**, 1081–1085.

2 X. Y. Zhou, B. R. Yu, Y. L. Guo, X. L. Tang, H. H. Zhang and W. S. Liu, *Inorg. Chem.*, 2010, **49**, 4002–4007.

3 C. F. Walker and R. E. Black, *Annu. Rev. Nutr.*, 2004, **24**, 255–275.

4 A. Takeda and H. Tamano, *BioMetals*, 2016, **29**, 177–185.

5 C. J. Frederickson, J. Y. Koh and A. I. Bush, *Nat. Rev. Neurosci.*, 2005, **6**, 449–462.

6 R. A. Colvin, A. I. Bush, I. Volitakis, C. P. Fontaine, D. Thomas, K. Kikuchi and W. R. Holmes, *Am. J. Physiol.: Cell Physiol.*, 2008, **294**, 726–742.

7 X. X. Chien, S. Zafra-Stone, M. Bagchi and D. Bagchi, *BioFactors*, 2006, **27**, 231–244.

8 M. Shyamal, P. Mazumdar, S. Maity, S. Samanta, G. P. Sahoo and A. Misra, *ACS Sens.*, 2016, **1**, 739–747.

9 M. L. Zastrow, R. J. Radford, W. Chyan, C. T. Anderson, D. Y. Zhang, A. Loas and S. J. Lippard, *ACS Sens.*, 2016, **1**, 32–39.

10 X. Zhou, P. Li, Z. Shi, X. Tang, C. Chen and W. Liu, *Inorg. Chem.*, 2012, **51**, 9226–9231.

11 B. Sandström, *Analyst*, 1995, **120**, 913–915.

12 G. J. Fosmire, *Am. J. Clin. Nutr.*, 1990, **51**, 225–227.

13 L. C. Costello, Y. Y. Liu, J. Zou and R. B. Franklin, *J. Biol. Chem.*, 1999, **274**, 17499–17504.

14 D. Noy, I. Solomonov, O. Sinkevich, T. Arad, K. Kjaer and I. Sagi, *J. Am. Chem. Soc.*, 2008, **130**, 1376–1383.

15 J. Chen and K. C. Teo, *Anal. Chim. Acta*, 2001, **450**, 215–222.

16 J. S. Becker, A. Matusch, C. Depboylu, J. Dobrowolska and M. Zoriy, *Anal. Chem.*, 2007, **79**, 6074–6080.

17 K. T. Kim, W. Heo, T. Joo and B. H. Kim, *Org. Biomol. Chem.*, 2015, **13**, 8470–8478.

18 J. Wu, W. Liu, J. Ge, H. Zhang and P. Wang, *Chem. Soc. Rev.*, 2011, **40**, 3483–3495.

19 Z. Guo, S. Park, J. Yoon and I. Shin, *Chem. Soc. Rev.*, 2014, **43**, 16–29.

20 H. Liu, X. Wan, T. Liu, Y. Li and Y. Yao, *Sens. Actuators, B*, 2014, **200**, 191–197.

21 Y. H. Lau, P. J. Rutledge, M. Watkinson and M. H. Todd, *Chem. Soc. Rev.*, 2011, **40**, 2848–2866.

22 W. K. Dong, X. L. Li, L. Wang, Y. Zhang and Y. J. Ding, *Sens. Actuators, B*, 2016, **229**, 370–378.

23 J. S. Wu, W. M. Liu, X. Q. Zhuang, F. Wang, P. F. Wang, S. L. Tao, X. H. Zhang, S. K. Wu and S. T. Lee, *Org. Lett.*, 2007, **9**, 33–36.

24 M. Kumar, A. Kumar, M. K. Singh, S. K. Sahu and R. P. John, *Sens. Actuators, B*, 2017, **241**, 1218–1223.

25 K. Gopaul, S. A. Shintre and N. A. Koorbanally, *Anti-Cancer Agents Med. Chem.*, 2015, **15**, 631–646.

26 S. Bawa, S. Kumar, S. Drabu and R. Kumar, *J. Pharm. BioAllied Sci.*, 2010, **2**, 64–71.

27 W. F. Lo, Y. W. Chou, C. H. Tseng, Y. H. Shiu, Y. W. Chen, S. C. Yang, Y. L. Chen, M. F. Lin and C. C. Tzeng, *Anti-Cancer Agents Med. Chem.*, 2015, **15**, 493–500.

28 J. J. Du, J. L. Fan, X. J. Peng, H. L. Li and S. G. Sun, *Sens. Actuators, B*, 2010, **144**, 337–341.

29 H. C. Ding, G. Liu, S. Z. Pu and C. H. Zheng, *Dyes Pigm.*, 2014, **103**, 82–88.

30 S. Heng, C. A. McDevitt, D. B. Stubing, J. J. Whittall, J. G. Thompson, T. K. Engler, A. D. Abell and T. M. Monro, *Biomacromolecules*, 2013, **14**, 3376–3379.

31 X. X. Zhang, R. J. Wang, C. B. Fan, G. Liu and S. Z. Pu, *Dyes Pigm.*, 2017, **139**, 208–217.

32 Y. L. Fu, C. B. Fan, G. Liu and S. Z. Pu, *Sens. Actuators, B*, 2017, **239**, 295–303.

33 S. Z. Pu, Q. Sun, C. B. Fan, R. J. Wang and G. Liu, *J. Mater. Chem. C*, 2016, **4**, 3075–3093.

34 S. Z. Pu, H. C. Ding, G. Liu, C. H. Zheng and H. Y. Xu, *J. Phys. Chem. C*, 2014, **118**, 7010–7017.

35 G. Li, D. B. Zhang, G. Liu and S. Z. Pu, *Tetrahedron Lett.*, 2016, **57**, 5205–5210.

36 Z. Y. Tian, S. Q. Cui, G. Liu, R. J. Wang and S. Z. Pu, *J. Phys. Org. Chem.*, 2016, **29**, 421–429.

37 E. M. Nolan, J. W. Ryu, J. Jaworski, R. P. Feazell, M. Sheng and S. J. Lippard, *J. Am. Chem. Soc.*, 2006, **128**, 15517–15528.

38 J. Mao, L. Wang, W. Dou, X. Tang, Y. Yan and W. Liu, *Org. Lett.*, 2007, **9**, 4567–4570.

39 X. Li, G. Liu and S. Z. Pu, *J. Phys. Org. Chem.*, 2014, **27**, 764–769.

40 E. J. Song, H. Kim, I. H. Hwang, K. B. Kim, A. R. Kim, I. Noh and C. Kim, *Sens. Actuators, B*, 2014, **195**, 36–43.

41 C. B. Fan, S. Z. Pu and G. Liu, *Dyes Pigm.*, 2015, **113**, 61–69.

42 T. Fukaminato, T. Doi, N. Tamaoki, K. Okuno, Y. Ishibashi, H. Miyasaka and M. Irie, *J. Am. Chem. Soc.*, 2011, **133**, 4984–4990.

43 K. K. Upadhyay and A. Kumar, *Org. Biomol. Chem.*, 2010, **8**, 4892–4897.

44 Z. Liu, C. N. Peng, Y. Wang, M. S. Pei and G. Y. Zhang, *Org. Biomol. Chem.*, 2016, **14**, 4260–4266.

45 Y. L. Fu, Y. Y. Tu, C. B. Fan, C. H. Zheng, G. Liu and S. Z. Pu, *New J. Chem.*, 2016, **40**, 8579–8586.

46 S. Q. Cui, Y. J. Tang, R. M. Lu and S. Z. Pu, *RSC Adv.*, 2016, **6**, 107475–107482.

47 G. J. Park, Y. J. Na, H. Y. Jo, S. A. Lee, A. R. Kim, I. Noh and C. Kim, *New J. Chem.*, 2014, **38**, 2587–2594.

48 L. Zhou, Y. Lin, Z. Huang, J. Ren and X. Qu, *Chem. Commun.*, 2012, **48**, 1147–1149.